Mutation Research 711 (2011) 28–40

Contents lists available at ScienceDirect

Mutation Research/Fundamental and Molecular Mechanisms of Mutagenesis

journal homepage: www.elsevier.com/locate/molmut
Community address: www.elsevier.com/locate/mutres

Review

Track structures, DNA targets and radiation effects in the biophysical Monte Carlo simulation code PARTRAC

Werner Friedland[a,*], Michael Dingfelder[b], Pavel Kundrát[a], Peter Jacob[a]

[a] Helmholtz Zentrum München, German Research Center for Environmental Health, Institute of Radiation Protection, Ingolstädter Landstr. 1, 85764 Neuherberg, Germany
[b] Department of Physics, East Carolina University, Greenville, NC 27858, United States

ARTICLE INFO

Article history:
Received 16 October 2010
Received in revised form 18 January 2011
Accepted 22 January 2011
Available online 31 January 2011

Keywords:
Modelling
Track structure
Multi-scale
DNA damage
DNA repair

ABSTRACT

This review describes the PARTRAC suite of comprehensive Monte Carlo simulation tools for calculations of track structures of a variety of ionizing radiation qualities and their biological effects. A multi-scale target model characterizes essential structures of the whole genomic DNA within human fibroblasts and lymphocytes in atomic resolution. Calculation methods and essential results are recapitulated regarding the physical, physico-chemical and chemical stage of track structure development of radiation damage induction. Recent model extension towards DNA repair processes extends the time dimension by about 12 orders of magnitude and paves the way for superior predictions of radiation risks.

Contents

* Corresponding author. Tel.: +49 89 3187 2767; fax: +49 89 3187 3363.
E-mail address: friedland@helmholtz-muenchen.de (W. Friedland).

0027-5107/$ – see front matter © 2011 Elsevier B.V. All rights reserved.
doi:10.1016/j.mrfmmm.2011.01.003

1. Introduction

Health risks to humans due to exposure to ionizing radiation continue to be an important issue although adverse radiation effects are meanwhile known for more than a century. Cancer is considered the major long-term contributor to health risk at levels below those causing acute tissue injuries [1]. Epidemiological studies provide the basis for estimating risks of radiation exposure to humans; however, the lack of statistical power is a fundamental limitation for risk estimation after low doses and dose rates [2]. Hence it is necessary to extrapolate the statistically significant epidemiological data from higher doses and dose rates down to the levels of background radiation and particular exposures under investigation. Extrapolations are needed also for irradiation conditions different from those where epidemiological data are available, as in the case of a manned Mars mission. For optimized use of beneficial radiation effects (e.g. radiation therapy of cancer) and protection against harmful effects, detailed understanding of the action mechanisms is necessary. Mechanistic modelling studies, benchmarked against available data, help understand the underlying processes both qualitatively and quantitatively, and may be used for knowledge-based extrapolations. Monte Carlo track structure simulations of ionizing radiation supplemented by mechanistic modelling of biological effects and consequences of this insult provide a bottom-up approach from first principles aimed at testing hypotheses on radiation action and response mechanisms. In combination with top-down modelling of cancer induction [3] and simulations on relevant intercellular signalling processes as in [4,5], the hierarchy of mechanistic modelling tools has the potential to allow improved predictions on radiation risks for low dose, low dose rate and exposure conditions for which no direct epidemiological data are available.

During the last decades a wide variety of track structure codes, reviewed in reference [6], have been developed and used in investigations of radiation effects. The present review article is focused on the PARTRAC suite of Monte Carlo codes and its application to radiation-induced biological effects. Originating from a track structure code for electrons in water vapour [7,8] it was step-by-step extended by photon interactions and DNA targets models of double-helix and chromosomes [9], chromatin fiber models in atomic resolution [10], liquid water cross sections [11] and stochastic chemistry calculation [12], track structures within heterogeneous targets [13], cross sections for ion interactions [14] and simulations of radiation damage to DNA by ions [15–17] and recently by a stochastic model of DNA double-strand break (DSB) repair via the non-homologous end-joining (NHEJ) pathway [18].

PARTRAC consists of different modules with defined data interfaces (Fig. 1) describing individual stages of radiation interaction and radiation response. The modules refer to separate programme codes written in FORTRAN. Thus, calculations of track structures or radiolytic processes can be performed and analysed independent from DNA targets [19,20]. The modular structure also allows easy expansion of the programme suite to include new effects and resources. In the following, basic methods of the different PARTRAC modules and essential results of PARTRAC calculations are reviewed.

2. Track structures in PARTRAC

2.1. Physical stage of track structure calculation

The physical stage of track structure simulations describes the transport of radiation, the local energy depositions, and the generation of ionized and excited atoms and molecules in the medium. According to the classical trajectory picture, Monte Carlo track structure simulations follow the primary particle as well as all produced secondary particles in an event-by-event manner, from starting or ejection energy down to total stopping. These calculations depend on reliable interaction cross sections of the primary and secondary radiation with the matter under consideration. Currently, PARTRAC is able to simulate photon, electron, proton, alpha particle and ion tracks in liquid water; these modules are reviewed in the following. A more general introduction to Monte Carlo transport techniques and sampling methods is given in references [7,21].

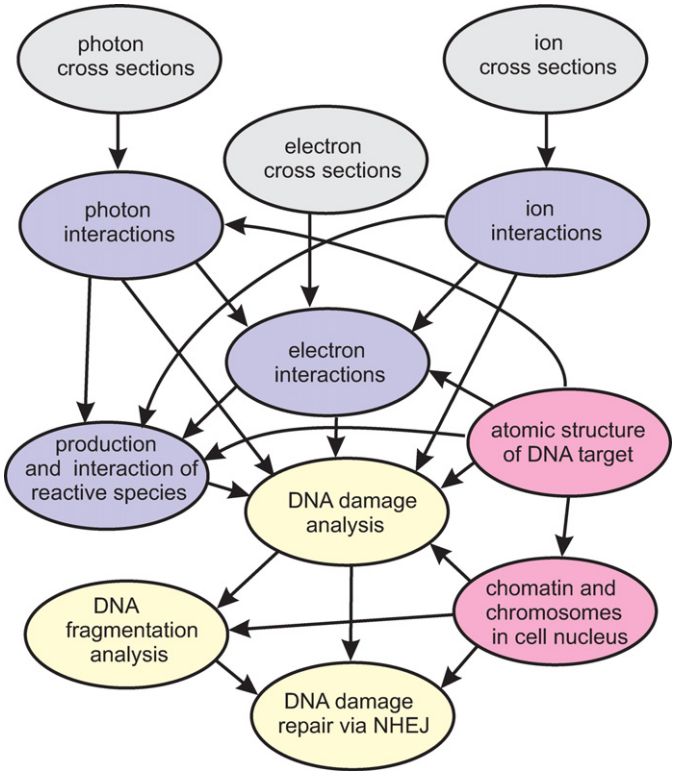

Fig. 1. Modules of PARTRAC and their interaction. Modules on DNA target structures (red) and cross sections (gray) provide input data for the track structure part (blue) and the biological effect part (yellow).

2.1.1. Photons

Photon transport in PARTRAC is modelled using atomic cross sections taken from the EPDL97 data library [22]. Coherent scattering, photoelectric effect, Compton scattering and pair production as well as Auger electron and fluorescence photon emission as relaxation processes are considered. Cross sections for liquid water or other biologically relevant materials are calculated from atomic cross sections using the additivity rule and density scaling; for details on the calculation and evaluation see e.g. the PENELOPE handbook [21]. Created secondary electrons are processed by the electron transport module.

2.1.2. Charged particles

Interaction cross sections for fast charged particles are conventionally obtained within the plane-wave Born approximation (PWBA). The PWBA is a first-order perturbation theory and anticipated to be valid only for sufficiently fast projectiles as compared to the velocities of atomic electrons. Within the PWBA the doubly differential (in energy transfer E and momentum transfer $\hbar k$) cross section factorizes in the generalized oscillator strength (GOS) of the target element and a purely kinematical factor. Since most

considered target materials are in the condensed phase it is usual to use the macroscopically defined inverse mean free path (IMFP) $\Sigma = N\sigma$ instead of the atomic cross section σ, where N is the number density of the considered material [23]. In this case the (complex) dielectric response function (DF) $\varepsilon(E, \hbar k)$ replaces the GOS. The DF of liquid water can be modelled and adjusted/fitted to two sets of experimentally obtained values: the optical reflectance measurement of Heller et al. [24] and the measurement by Hayashi et al. [25] using synchrotron radiation. PARTRAC uses a more conservative approach and models the DF of liquid water as a superposition of Drude-like functions and adjusts parameter to the measurements of Heller et al. [24] and theoretical constraints. This model considers five excited states (two electronic excitations $\tilde{A}^1B_1$ and B^1A_1, two Rydberg states Ryd A + B and Ryd C + D, and diffuse bands) and five ionization shells (labelled $1b_1$, $3a_1$, $1b_2$, $2a_1$, and K-shell of oxygen). The model is documented in detail in references [11,26]. Other models including those using the newer experimental data of Hayashi et al. [25] are described in references [27,28]. The Bethe approximation is asymptotic to the PWBA and is often used for relativistic particle energies. The Bethe approximation takes advantage of binary collisions and averages over momentum transfers in this limit. The (single) differential (in energy transfer) IMFP in the Bethe approximation also relies on the dielectric response function but needs only optical data, i.e. for momentum transfer $\hbar k = 0$. This allows for much easier calculations of interaction cross sections.

Semi-empirical approaches are another possibility to calculate interaction cross sections. They are often used outside the validity of the first Born or Bethe approximations, especially for low-energy electrons. Semi-empirical models rely on simple mathematical relationships between the key quantities and are typically fitted to (scarcely existing) experimental data and extrapolated to other target elements and energy regions. In the following the transport models for charged particles currently implemented into PARTRAC are described.

2.1.2.1. Electrons. Currently, PARTRAC is able to simulate electron tracks from 10 eV up to 10 MeV. Interaction cross sections for the considered five excitations and five ionization levels are obtained within the PWBA using the above mentioned model for the dielectric function of liquid water. For electrons above 10 keV the relativistic Bethe approximation is used. For electrons below 500 eV a semi-empirical correction factor is added to account for non-Born effects. Electron exchange is also considered using a semi-empirical model. Elastic scattering is taken into account, too. Details to the cross section calculations are given in references [11,26].

To assess the validity of approximating cell nuclei and genomic DNA by liquid water, the influence of inhomogeneous targets on radiation-induced DNA damage was investigated [13]. To this end, electron impact ionization cross sections were calculated for constituents of the DNA [29], i.e. the bases adenine, cytosine, guanine and thymine and the sugar-phosphate backbone. Two alternative algorithms were used; they yielded similar total electron ionization cross sections but their predictions differed when cross sections per molecular orbital were compared. For incoming electron energies above 250 eV the cross sections for DNA of the two formalisms were in good agreement with the cross section for liquid water [11]. However, in the energy range below 250 eV, the larger first ionization potential of liquid water leads to smaller ionization cross section in water than in DNA. Nevertheless, the impact of this difference on calculated radiation damage to DNA was limited [13] (see Section 3.2).

Currently, the electron cut-off energy in PARTRAC is 10 eV. Electrons with kinetic energy less than 10 eV (including secondary electrons with emission energies below this cut off value) are stopped at their current position and their remaining energy is deposited locally. Recently, the electron transport model in PARTRAC has been extended to simulate electron transport down to 1 eV by including low-energy phonon, vibrational and electronic excitations as measured by Michaud et al. [30]. The new transport model is documented in reference [31] and is currently evaluated by simulating new experimental data obtained from measuring secondary electron emission yields from thin foils of amorphous ice [32]. This new model has not yet been used in simulations of a biological endpoint with PARTRAC.

2.1.2.2. Protons and alpha particles. The proton and alpha particle transport model of PARTRAC is able to simulate protons and alpha particles with kinetic energies up to 1 GeV. The low energy cut off is set to 1 keV. The transport model considers excitations, ionizations, and the charge changing processes of electron capture and loss. Elastic scattering is not considered. Ionization and excitation cross sections above 1 MeV total energy are calculated using the same (non-relativistic) PWBA and Bethe approximations as for electron transport [14,16]. Below 1 MeV kinetic energy, semi-empirical models based on the Rudd model are used. At these energies the proton can pick up an electron (electron capture) and become a neutral hydrogen atom; this neutral hydrogen atom itself can lose its electron (electron loss), which is emitted in forward direction with the same velocity as the proton. Both electron capture and electron loss processes as well as ionization and excitation cross sections of neutral hydrogen are modelled using semi-empirical models based on available experimental data on water vapour and theoretical predictions, see reference [14] and regarding secondary electron emission spectra [23]. In case of alpha particles, three charge states (He^{2+}, He^{+}, and neutral helium He^0) as well as one and/or two electron loss and capture processes need to be considered. Recommended stopping cross sections [33] are used to adjust parameter sets of the adopted semi-empirical models [16,34]. At higher energies (beyond 1 GeV) the Fermi-density effect needs special consideration [14,35].

2.1.2.3. Light and heavy ions. PARTRAC can simulate bare ions (heavier than helium) with atomic number Z from about 1 MeV/u to 1 GeV/u using the velocity and charge scalability of proton cross sections within the PWBA and Bethe approximation. The doubly differential IMFP for a heavy ion of velocity v is given by Z_{eff}^2 times the doubly differential IMFP for a proton of the same velocity v. The effective charge Z_{eff} is obtained from the Barkas formula: $Z_{\mathrm{eff}} = Z(1 - \exp(-125Z^{-2/3}\, v/c)$ [36] where c is speed of light. Multiple ionizations and charge changing events are not considered. Secondary electron emissions are modelled by the same semi-empirical model as for protons but applied to the heavy ion.

2.2. Physico-chemical stage of track structure calculation

Ionized and excited water molecules produced during the physical stage are rather transient states which decay rapidly and thereby form the chemical species •OH, H•, •O•, H_3O^+ and H_2; in accord with other modelling approaches [37–39] this process is assumed to occur within 1 ps. Electrons below 10 eV, including those produced by auto-ionization of excited states, come to rest during this time interval and become solvated as hydrated electrons (e_{aq}^-) by attachment of water molecules which hinder immediate recombination. Modelling of this physico-chemical stage in water is determined by the decay channels, their branching ratios and by the positions of the produced species and hydrated electrons which were first set-up for electron tracks [12] considering assumptions and parameters adopted by other model approaches. In a reassessment in view of radiolysis after high-LET irradiation [20] new data on the dependence of the mean thermalization dis-

tance of sub-excitation electrons on their energy [40] have been taken into account.

Processes during the physico-chemical stage are: an ionized water molecule reacts quickly with a nearby H_2O molecule to form a H_3O^+ ion and an $^\bullet OH$ radical as the solely possible channel. For excited water molecules, depending on their type, three pathways are distinguished: (i) relaxation to the ground state without production of reactive species, (ii) dissociative decay processes forming either the radicals $^\bullet OH$ and $H^\bullet$, or H_2 and the bi-radical $^\bullet O^\bullet$ which is assumed to interact immediately with a water molecule leaving behind two $^\bullet OH$, and (iii), provided that the excitation energy is above the ionization threshold of 10.79 eV, auto-ionization processes which are modelled like other ionizations plus e_{aq}^- formation. As in similar studies, fixed decay channels independent from radiation quality have been used for excited and ionized water molecules, resulting in rather ion- and LET-independent initial yields for all reactive species [20]. However, experimental data for 10 MeV C ion irradiation showed, compared to γ-rays, 30% reduction of e_{aq}^--yields after 5 ps [41]. This may indicate also an overestimation of $^\bullet OH$ yields after high-LET irradiation due to neglecting fast recombination processes, and opens prospects for future model improvements.

2.3. Chemical stage of track structure calculation

During the chemical stage of track structure development, the initially rather non-homogeneously distributed species $^\bullet OH$, H_3O^+, $H^\bullet$, H_2 and e_{aq}^- react with each other and the newly formed species OH^- and H_2O_2 under ubiquitous presence of water molecules, and undergo diffusive Brownian motion. After about 1 μs an almost homogeneous distribution of residual species is obtained and their concentration approaches a limiting value. In a nutshell, the species $^\bullet OH$, H_3O^+, $H^\bullet$ and e_{aq}^- are consumed whereas H_2, OH^- and H_2O_2 are produced within this phase. Consumption and production depend considerably on the initial distribution of species given by the quality of the initiating radiation.

The chemistry module of PARTRAC describes the process of radiolysis in oxygen-free water. It follows a step-by-step algorithm which has also been adopted by other investigators [37,39,42]. Diffusion is represented by jumps of species in randomly selected directions. After each diffusion step, a scan for reaction partners is performed based on reaction radii R that are determined from the observed reaction rate constants k assuming partially diffusion-controlled reactions [43] according to $k = 4\pi D' R^2/(R + (\pi D' \Delta t)^{0.5})$ where $D' = D_A + D_B$ is the relative diffusion coefficient for reactions between species A and B and Δt is the time step used in the simulation. Upon reaction the reactants are replaced by the respective chemical products. As the time interval of interest spans six orders of magnitude, the adopted time step can be increased during the simulation, typically from 0.1 ps to 30 ps, to ensure sufficient time resolution in the initial part and reasonable computing times at the end of the chemical stage. Time-step dependent diffusion hops and reaction radii, complemented by jump-through corrections [44], provide time-step independent reaction kinetics. Parameter selection for diffusion and reactions during the chemical stage resulted in good agreement between calculations and various experimental results for the time dependent yield of diverse species (e_{aq}^-, H_2, $^\bullet OH$, H_2O_2) after low-LET irradiation [12] as well as after photon, electron, proton, helium ion and carbon ion irradiation, covering an LET range from 0.2 up to 750 keV/μm [20] where both the time- and the LET-dependences of the calculated yields of species were found in accord with experimental and theoretical data from the literature. Thus, the simulation of the physico-chemical and chemical stage in PARTRAC can be regarded as a sound basis for modelling of indirect DNA damage induced by free-radical attacks.

3. Modelling of DNA targets in PARTRAC

About five decades ago the hypothesis was raised that it is the nuclear DNA which is the target whose damage by ionizing radiation leads to manifestations of radiation effects such as arrest of cell division, chromosomal aberrations, mutation and cell-death [45]. Damage to genomic DNA is still supposed to be the main initiating event by which radiation causes long-term harm to organs and tissues of the body damage [46]. This conventional paradigm for radiobiology based on target theory, however, could not explain the experimental observation of "non-targeted effects", most notably genomic instability [47] and the bystander effect [48], and therefore the need for a new paradigm has been proposed [49]. The contribution of these phenomena to radiation harm on tissue and organ level, and their impact on radiation risk will continue to be an important issue, also regarding modelling approaches [3,4]. Nevertheless, these emerging phenomena are likely to complement rather than replace the role of DNA as a critical target for radiation-induced biological effects.

3.1. Representation of DNA structures

DNA in a human cell nucleus is structured on a variety of levels including DNA double-helix, nucleosomes, chromatin fibers, fiber loops, chromatin domains, and chromosomes. It has to be expected that these structures have, depending on the end point, significant impact on radiation-induced biological effects. The consideration of structural levels ranging from the DNA double-helix in atomic resolution up to chromosomes referring to human fibroblast or lymphocyte nuclei in G0/G1 state has governed DNA modelling approaches in PARTRAC. Aspects of DNA target dynamics and cell-cycle dependence of DNA structures are not yet adequately taken into account in our modelling approaches; first steps towards this issue have been made regarding their impact on the outcome of DNA repair processes [18].

Historically, first considerations of DNA target sizes were introduced by the concept of microdosimetry [50–52] which was developed to establish a framework for assessing radiation effects on cellular and sub-cellular scales. On such a basis, energy deposition patterns were studied in small cylindrical volumes representing pieces of the DNA double-helix, nucleosomes and chromatin fiber segments [53,54]. The first model of a DNA double-helix used for calculations of SSBs and DSBs consisted of a cylinder of 2.3 nm diameter cut into sections of 0.34 nm thickness representing nucleotide pairs; this cylinder was divided into an inner cylinder of 1 nm diameter and two surrounding arcs rotated by 36° per nucleotide pair in order to separate the bases from the sugar-phosphate backbone [55]. This DNA model has been used in several studies on initial single-strand break (SSB) and DSB yields, strand break complexity [39,56], contributions of direct and indirect effects [57], and it was also implemented in an early PARTRAC version [9]. In the 1990s, DNA models have developed in two respects: an atomic description of the DNA double-helix [58] and its arrangement in nucleosomes [59] on the one hand, and the representation of higher-order structures on the other hand [60,61]. Both ideas were combined into a chromatin fiber model with atomic resolution [62], later including variations in compactness and nucleosome orientation [63].

The first DNA target model in PARTRAC with atomic resolution described a flexible arrangement of nucleosomes within a 30-nm chromatin fiber or a zig-zag formation and their connection by linker DNA segments [10]. Basic fiber elements were defined under the boundary condition that the structure reiterated identically with a certain shift along the fiber axis after a predefined number of nucleosomes, e.g. 6 nucleosomes in one solenoidal turn along 11 nm or 30 nucleosomes in stochastic crossed-linker arrangement

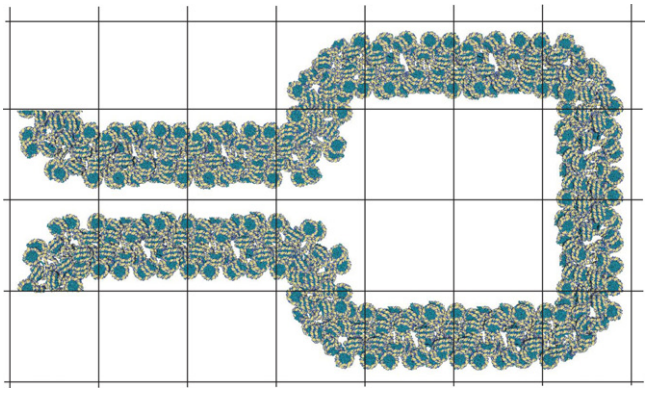

Fig. 2. Illustration by POV-Ray™ raytracer software of flat chromatin fiber loop of about 100 kbp genomic length constructed from 18 basic elements on a grid of 50 nm × 50 nm.

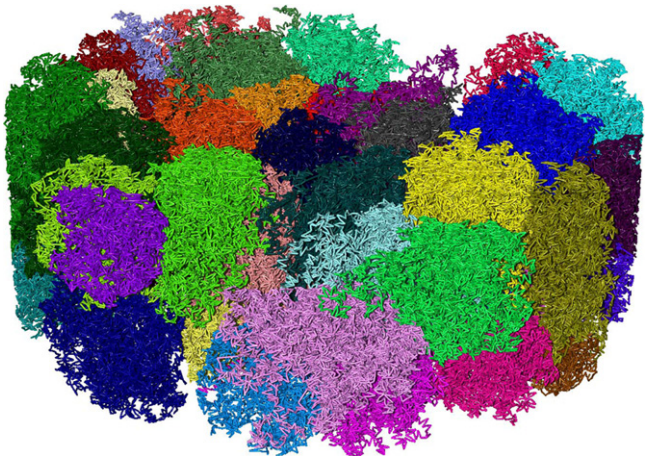

Fig. 3. Illustration by POV-Ray™ raytracer software of chromatin fibers of 46 chromosomes of a human fibroblast cell nucleus. Different colors represent different chromosomes.

along 50 nm. This principle has been retained during further model developments; it assured seamless connection of all lower-order structures when two basic elements were stacked in correct orientation on top of each other and allowed expansion of atomic resolution from coordinates within the basic elements towards higher-order DNA structures. Chromatin fiber loops were first constructed via bent fiber elements in which the cylinder around a basic element was transformed to a torus sector and the DNA inside correspondingly [10]. Later, an assembly of virtually linked linear fiber rods (where the sequence of nucleotide pairs at the top of one rod continues at the bottom of next one disregarding the gap in-between) of 18 kbp length represented a loop with a rhomb-like form, and seven specifically arranged loops represented chromatin domains of 500 kbp size [15]. In the most recent model version, five basic cubic elements of 50 nm × 50 nm × 50 nm size have been constructed, containing a straight fiber segment connecting the bottom and upper wall of the cube and four bent elements connecting the bottom wall with the other ones [64]. A flat chromatin fiber loop comprising 18 elements and about 100 kbp is presented in Fig. 2. Further chromatin model variants have been adopted for modelling studies on the effects of ultrasoft X-rays on linear DNA, nucleosomes and chromatin fiber pieces using an atomic representation of histones [13,65] and on the protective role of DNA higher-order structures against •OH radical attack [66] including a representation of SV40 minichromosomes.

As a first step towards representing whole chromosomes in PARTRAC, virtual linkage was used for a study of size distributions of DNA fragments [67]. Chromosomes within a human fibroblast cell nucleus in G0/G1 phase were constructed inside a cylindrical nucleus model with 15 μm diameter and 5 μm height, subdivided into 46 territories with volumes proportional to chromosomal lengths (Fig. 3). This and similar DNA target models have been used in several investigations on ion-induced radiation damage [16,17,68,69]. The most recent chromosome model [64] describes a human inter-phase cell nucleus of a lymphocyte with a spherical shape of 10 μm diameter and of a fibroblast with an ellipsoidal shape with axis lengths of 20 μm, 10 μm and 5 μm, both including a total genomic length of 6.6 Gbp. Each of the 46 human chromosomes is represented by an unbroken self-avoiding sequence of the aforementioned five basic elements with 50 nm side length. Distribution and structure of chromosomes are based on an arrangement of spherical chromatin domains (SCDs) [70]. The centers of 6070 SCDs are taken as anchor points for the generation of loop rosette structures [71] by departing the chromatin path from and reapproaching to the SCD centers until the associated genomic length of one megabasepair is assigned; then the path is directed towards the next SCD center. The resulting chromatin data base includes the sequence of locations, types and orientations of about 1.2 million basic elements that describe genomic DNA. In this way, a single representation of DNA structure in a cell nucleus is realized, which accounts for different levels of DNA architecture from the DNA double-helix up to chromatin domains in an inter-phase nucleus, and contains information about positions of all atomic constituents. However, only a single out of myriads potential DNA configurations is represented and aspects of chromatin dynamics are not considered, leaving room for future improvements of the DNA model in PARTRAC.

3.2. Interdependence between DNA target and track structure

PARTRAC calculations of radiation effects are usually based on a superposition of the DNA target model with track structures determined in liquid water. However, the presence of DNA in its conformation has some effect on track structures in the physical stage due to differences in cross sections, and even more in the physico-chemical and chemical stages due to the presence of other materials than water. The first issue has been studied in detail [13], taking into account the molecular and geometric structure of the DNA target in the interaction of photons and electrons by using ionizing cross sections for DNA constituents (cf. Section 2.1.2.1) [29]. Significant local inhomogeneities in dose and elevated yields of SSBs and DSBs due to direct effects were found for photon irradiation with energies between the carbon and oxygen K absorption edge (0.28–0.54 keV). Outside this photon energy range the results were rather similar to data obtained by superposition of track structures calculated in liquid water with a geometric model of the DNA target.

The target volume representing DNA and histones is formed by the union of atomic spheres. Using for these spheres reported values of van der Waals radii (0.12, 0.17, 0.15, 0.14 and 0.19 nm for H, C, N, O, P, respectively [72]) would generate a holey structure. Such artefacts are removed by adjusting the DNA and histone volume in the model to reported densities [73,74] via increasing the van der Waals radii of all atoms in DNA and histones (where H atoms are not included) by factors of 1.3 and 1.4, respectively [13]. Moreover, to account for the primary hydration shell surrounding cellular DNA [75], energy depositions inside the inner hydration shell of about 12–15 tightly bound water molecules per nucleotide are assumed to contribute to direct (as quasi-direct) effects, i.e. they are scored in PARTRAC like events within nearby DNA constituents and produced no reactive species during the physico-chemical stage. The inner hydration shell is represented in PARTRAC calculations by

including a layer of 0.16 nm around the DNA helix or by adopting an increased van der Waals radius multiplier of 2.

In the physico-chemical stage, reactive species are neither produced from energy depositions inside the volume occupied by DNA nor created within that volume due to nearby energy depositions. Interactions between DNA constituents (deoxyribose, adenine, guanine, cytosine and thymine) and •OH radicals or e_{aq}^- during the chemical stage are calculated like other reactions between species; reaction rates are derived from [76]. The lifetime of •OH radicals in the nuclear environment is considerably reduced due to the presence of further scavenging molecules whose overall scavenging capacity has been estimated at $4 \times 10^8\ s^{-1}$ [77]. Since these reactions are not explicitly included in the chemistry module of PARTRAC, additional removal of •OH species with a characteristic time of 2.5 ns is considered. In addition, histones are assumed to act as a radical scavenger, i.e. all species which diffuse into the volume of the union of histone atoms are removed from the calculation. The protective effect of histones and DNA folding on SSB and DSB induction has been studied in detail in [66].

4. Calculation of radiation effects in PARTRAC

4.1. DNA single-strand breaks (SSBs)

Within the spectrum of DNA lesions the importance of SSBs of the DNA double-helix is assumed to be low for late effects of radiation damage [78]. Nevertheless, their incidence is an essential issue in DNA damage modelling since calculations of the much more important DSBs are usually based on calculations of SSBs occurring on opposite strands in sufficient vicinity. Apart from some earlier investigations [10,56,79], model calculations of strand break induction distinguished between so-called direct effects from ionizations and other energy depositions to DNA on the one hand, and so-called indirect effects due to interactions of DNA with reactive species produced in the surrounding water during the chemical stage on the other hand. A clear-cut distinction between both contributions, however, is not possible; instead, the borderline between direct and indirect effects is usually drawn between non-scavengable strand breaks as direct effects which include interactions occurring within the inner hydration shell, and the other breaks which may be suppressed by the addition of an •OH radical scavenger in sufficient concentration as indirect effects.

The conditions under which SSBs are induced have to be parameterized in model calculations for both contributions, since simplifications of the DNA representation and the complexity of individual processes leading to strand breakage do not allow an ab-initio calculation of strand break yields without parameter adaptation. In the earliest work using annular DNA segments [55], measured strand breaks following ^{125}I decay were reproduced assuming that an energy deposition above a threshold of 17.5 eV in one sugar-phosphate volume resulted in a strand break; further induction of breaks from •OH radical attack was not considered. This result was confirmed in calculations of strand breaks after electron, proton and alpha particle irradiation [56], and used in subsequent investigations based on that DNA model [57,80] although there additional induction of DNA strand breaks by •OH attack was taken into account. First PARTRAC calculations of strand break induction using a DNA model with atomic resolution adopted energy deposition thresholds slightly above 10 eV; however, these rather low values were due to negligence [10] or underestimation [67] of SSBs from indirect effects. Measurements of DNA strand break induction by electrons [81] and photons [82] down to about 5 eV energy have initiated a revision of the strand break calculation in PARTRAC: linear increase of the break induction probability from 0 at a threshold energy deposition of 5 eV with increasing energy deposit in one sugar-phosphate group has been adopted up to an energy parameter value for (and above) which the probability equalled 1. These energy parameters have been selected in view of the envisaged number of strand breaks per gray and cell after low-LET irradiation such as ^{60}Co γ- or 220 kVp X-rays. Based on the total yield of about 1000 per Gy and cell [83], and a ratio of 35:65 between direct and indirect effects [84], about 350 strand breaks from direct effects have to be expected, and a corresponding yield was obtained in calculations using 37.5 eV [15–17,64,85] or 40 eV [66,68,69,86] as energy parameter. A higher parameter value of 57.6 eV has been used for calculations considering the influence of DNA on track structures [13] and those excluding heat-labile sites from strand breakage [18].

With respect to strand break induction due to indirect effects after low-LET irradiation, the calculated yields have been found in agreement with the abovementioned experimental data when 65% of the •OH interactions with deoxyribose lead to SSBs. This fraction corresponds to 13% of all •OH-DNA interactions, a value used in other modelling studies [57], since 20% of the interactions of •OH with DNA constituents react with deoxyribose, and about 80% are base attacks.

The calculated dependence of the SSB yield on initial photon energy shows a rather slight minimum around about 1 keV [13], resulting from a reduced contribution of indirect effects around that energy and an invariant yield from direct effects. Rather constant SSB yields from direct effects and decreasing yields with increasing LET due to indirect effects have been obtained after proton irradiation [15]. Other calculations of SSB yields have revealed a smaller decrease with increasing LET or decreasing particle energy of protons and α particles [57], see also reference [87]. For filtered 220 kVp and 29 kVp X-rays, slight reductions by 1% and 3%, respectively, have been obtained in comparison to ^{60}Co γ-rays [88]. DNA compactness has been found to have significant impact on the SSB yield due to indirect effects after photon irradiation; the calculated protection of a 30-nm chromatin fiber compared to a DNA double-helix reduced the SSB yield by factors of 2 [13] and 2.6 [66]. Considerably more pronounced effects of DNA conformation in experiments yielding a factor of 100 [89] may indicate that the generation of unfolded and histone-depleted DNA in the experiments might have been associated with a drastic reduction of the scavenging capacity for •OH radicals [66].

4.2. DNA double-strand breaks (DSBs)

The induction of DSBs is determined in PARTRAC from the yield of breaks on opposite strands within a maximum genomic distance. Usually 10 bp is adopted as a threshold value, but also other values and their influence on DSB yields have been considered [10,56]. DSB induction from two SSBs should reveal an enhanced energy threshold for this endpoint compared to SSB induction, however, intriguing experimental results have been found in studies of SSB and DSB induction after low-energy photon and electron irradiation: DSBs could be produced by photons well below 10 eV [90] and photon-energy dependent action spectra for SSBs and DSBs were rather parallel [82]. A transfer of radical sites from one broken strand to the opposite strand and subsequent cleavage has been proposed as a mechanism in which a single interaction with DNA may lead to a DSB [91]. In response to these findings, a transfer into DSBs of 1% of SSBs induced by either direct or indirect effects has been introduced in PARTRAC [13] and adopted in subsequent calculations.

For ^{60}Co γ-irradiation of human cells, absolute DSB yields between 8 and 9 DSB per Gy and 10^9 base pairs (Gbp) and a SSB:DSB ratio of about 20:1 result from the SSB parameter selection (see Section 4.1), 10 bp maximum distance between the strand breaks and

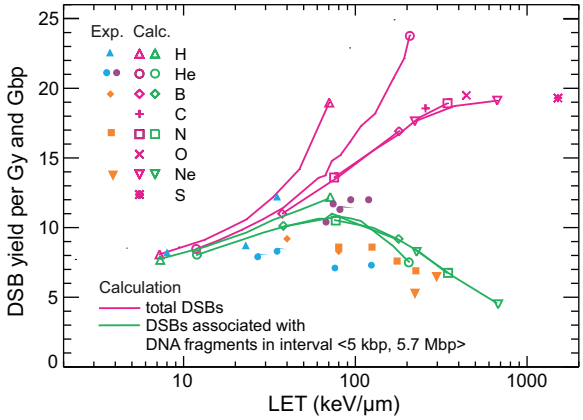

Fig. 4. Induction of DSBs due to irradiation with various ions as a function of LET. Magenta lines and symbols: calculated total DSBs; green lines and symbols: calculated DSBs associated with DNA fragments in size interval 5 kbp to 5.7 Mbp; cyan symbols: experimental results for H and He ions [95]; violet symbols: experimental results for He ions [96]; orange symbols: experimental results for B, N and Ne ions [97,105].

1% SSB to DSB transfer [15,67]. This SSB:DSB ratio corresponds to experimental findings [89], and the DSB yield is within the range of experimental data [92]: about 10 per Gy and Gbp derived from fragment analysis after X-ray irradiation, and between 2.6 and 7.7 per Gy and Gbp obtained by other techniques.

Calculated DSB induction after irradiation with various photon radiation qualities [13,67] shows an increasing trend with decreasing photon energy in agreement with other model calculations [88], both yielding about 10% more DSBs after filtered 220 kVp X-rays compared to ^{60}Co γ-rays, and experimental results [93]. However, the calculated DSB yield for C_K ultrasoft X-rays (0.28 keV) does not exceed the corresponding result after Al_K (1.5 keV) irradiation, and the calculated RBE values of 1.6 for both radiation qualities is below the measured result of 2.7 and 1.9 for C_K and Al_K, respectively. This difference may be related to the dose inhomogeneity and/or the enhanced photo-absorption after C_K irradiation by interactions with phosphate L-shell electrons (more than 40% of photon interactions) compared to Al_K irradiation (less than 10%).

The calculated DSB yield after ion irradiation of human fibroblasts increases with increasing LET (Fig. 4) [15–17]. For protons the yield is higher than for helium ions of the same LET, and for both particle types the increase continues up to the maximum possible LET values; these findings agree with other model calculations [94]. For heavier ions (B, C, N, O, Ne, S) the DSB yields are lower than for helium ions of the same LET and tend to saturate above about 300 keV/μm, whereas differences between ion types are negligible. Corresponding experimental results show a similar LET dependence only after proton [95] and partly after helium ion irradiation [96]; other measurements report an almost constant or decreasing trend after irradiation with He [95], N, B and Ne ions [97]. The essential difference between these results and the calculations is the experimental limit in the detection of DSBs associated with small fragments which increase steeply with increasing LET. The reduced disparity for the measurements after helium ion irradiation results from inclusion of DNA fragments down to 0.1 kbp [96]. However, adopted methods of DSB yield determination from measurements of DNA fragments in a certain size interval can be reproduced in PARTRAC model calculations. This procedure removes essentially the discrepancy in the trend for boron, nitrogen and neon ions, where the experimental yield has been determined from DNA fragments in the size interval between 5 kbp and 5.7 Mbp [97]. These results emphasize the necessity of considering the non-random DSB distribution for the determination of DSB yields after ion irradiation and give a consistent explanation for the reported low DSB yields after high-LET irradiation [92].

4.3. DNA fragment distributions

The complete hierarchy of DNA structures on all size scales in the DNA target model allows calculations of DNA fragment distributions over the full size range from a few base pairs up to chromosomal size. Size distributions of DNA fragments reveal, unlike SSBs and DSBs, in general non-linear dose dependence. Two important aspects are related to radiation-induced DNA fragment distributions: on the one hand they reflect essential characteristics of DNA organisation within the cell nucleus that are independent from incident radiation qualities. On the other hand they highlight features of incident radiation track structures.

The first aspect was highlighted by the detection of a peak in measured DNA fragment size distributions at about 80 bp which corresponds to one turn of the DNA helix around a nucleosome [98]. Model calculations reproduced this nucleosomal peak in great detail [13,63]. Furthermore, calculated DNA fragment distributions in the size range up to 3 kbp were found to be rather independent on incident electron energy and single- and double-stranded DNA fragment distributions were quite similar but specific regarding the underlying chromatin fiber structure [10]. These chromatin-related peaks in DNA fragment distributions are generated by two DSBs in close spatial vicinity resulting from a single track, whereas for DNA fragment sizes below 1 kbp the contribution due to DSBs from two independent tracks was found to be negligible up to doses of several hundred Gy [67]. Measured DNA fragment distributions in that size range [99] were inconsistent with calculated distributions for an assumed solenoidal structure of the chromatin fiber [62]. Refined experimental DNA fragment size distributions were in accord with a chromatin fiber model in zig-zag structure [63]. However, to obtain a density of 5.9 nucleosomes per 11 nm fiber length derived from X-ray and neutron scattering experiments [100,101], the zig-zag structure has to be compressed; this yields, after some twist to avoid overlapping of nucleosomes, a crossed-linker formation. Such crossed-linker structure of the chromatin fiber has been adopted in further PARTRAC studies with stochastic positioning of 5.4–6 nucleosomes per 10 nm fiber length. Despite this stochasticity within the building blocks of the fiber, the continuous repetition of spatial vicinity relations for certain genomic distances gives rise to pronounced peaks in the distributions of short DNA fragments [64], whereas experimental data revealed not more than four indistinct peaks below 0.5 kbp DNA fragment size [63]. Calculations using larger sets of basic chromatin fiber elements are supposed to solve this discrepancy, as indicated by the modelling studies in reference [63].

The second aspect, the radiation quality dependence of DNA fragmentation patterns is closely linked to deviations from a random distribution of DSBs along the genome. DNA fragment distributions resulting from randomly distributed DSBs are fully determined by the number of DSBs with minor influence of chromosomal sizes at low numbers of DSBs [102]. First non-random DNA fragment distributions were reported for nitrogen and iron ions with about 100 and 150 keV/μm LET, respectively [103], and after α particle irradiation [104]. In both studies, small deviations from random DNA fragment distributions were also found after X-ray irradiation, and resulted in a higher DSB yields from DNA fragment analysis compared to its determination based on the random breakage model. Later, for nitrogen ions with LET values above 80 keV/μm peaks were detected at 50–200 kbp in the fragment distributions [105], whereas only minor fluctuations from the random distribution were observed for ^{60}Co γ-irradiation with 150 Gy. A study of DNA fragment size distributions after pro-

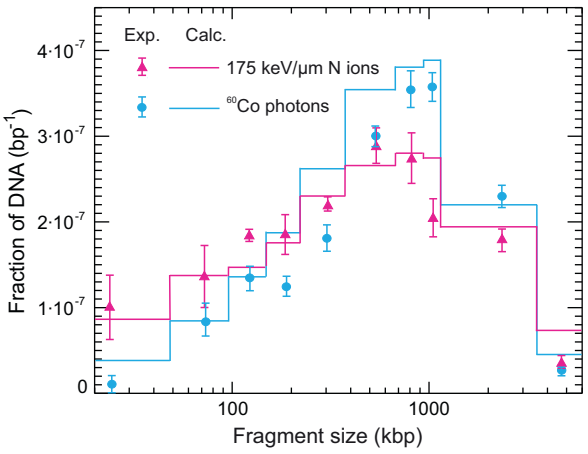

Fig. 5. Fraction of DNA in fragment size intervals as a function of mean fragment size. Magenta: data for 175 keV/μm nitrogen ions with a fluence of 5 particles per μm^2 (140 Gy); cyan: data for ^{60}Co γ-irradiation with a dose of 150 Gy, symbols: experimental results [105], lines: calculations.

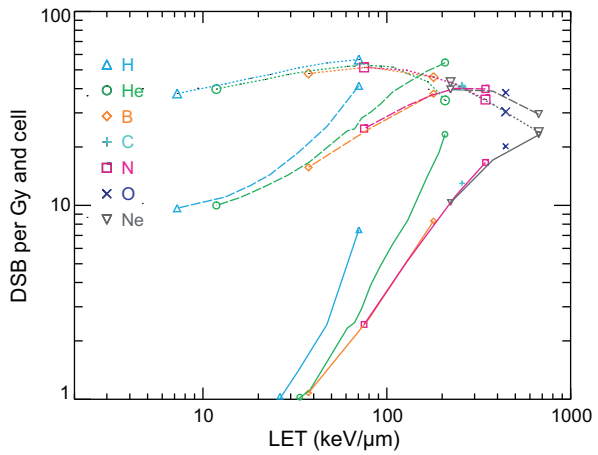

Fig. 6. Calculated yield of DSBs and DSB clusters of various complexity as a function of LET. Dotted lines and large symbols: *DSB* (DSBs without further nearby DNA strand breaks); dashed lines and midsize symbols: *DSB*$^+$ (DNA damage clusters with one DSB and at least one SSB); solid line and small symbols: *DSB*$^{++}$ (DNA damage clusters with at least two DSBs).

ton and helium ion irradiation compared to ^{60}Co γ-irradiation revealed that a random breakage model could describe with a reasonable approximation the DNA fragmentation induced by γ-rays, whereas the chromatin organization at the loop level was proposed to affect the production of fragments in the 0.02–1 Mbp region [106].

Model calculations on DNA fragment distributions in the size range above 10 kbp represent a test of the DNA target model structures of corresponding lengths. Calculations for Al_K and 220 kVp X-rays and ^{60}Co γ-rays have yielded no deviation from random-breakage, whereas for C_K ultrasoft X-rays enhanced yields of small fragments have been attributed to the inhomogeneous dose distribution within the cell nucleus [13,67]. For proton irradiation, calculated fragment size distributions deviate significantly from random breakage distributions above an LET of 10 keV/μm [15], and at 28.5 keV/μm LET measured and calculated fragment distributions have been found in agreement [107]. For α particle irradiation, the elevated production of DNA fragments in the size range 10–100 kbp after 100 Gy [104] has been reproduced in calculations [16]. After nitrogen ion irradiation, the increasing deviation with increasing LET of measured DNA fragment distributions from random breakage behaviour obtained after ^{60}Co γ-irradiation [105] has also been obtained in calculations (Fig. 5) [64]. Reasonable agreement between experiment and calculation in further studies on DNA fragmentation induced by ^{56}Fe ions [69,86] has motivated predictions of the radiation quality dependence of DNA fragmentation spectra with PARTRAC [68]; this study also emphasized the contribution of DSB associated with experimentally undetected small fragments to the DSB yield.

Further calculations of non-random DNA fragment distributions have been reported for a size scale from a few 10 kbp to a few Mbp based on combinations of DNA target and track structure models [108] as well as simply on chromatin models [109–111]. A major issue in the analysis of radiation-induced DNA fragment size distributions was the background fragment distribution obtained by application of the experimental protocol to unirradiated cells. Whereas PARTRAC studies for proton-induced DNA fragmentation revealed that simple subtraction of the background distribution from the measured distribution produces a negligible error [15], it has been proposed that this method may lead to incorrect estimation of DNA breakage frequencies, and alternative approaches have been developed [112–114]. This issue is closely related to the origin of background fragments and its interference with radiation-induced production; these largely unknown mechanisms may depend on cell types, experimental protocols and other conditions, and therefore a general necessity for sophisticated background correction is not evident.

4.4. Strand break complexity

Cell inactivation experiments with ultrasoft X-rays and ions, coupled with theoretical track structure analyses, emphasized the biological importance of localized track features over nanometer dimensions, and suggested that the stochastic clustering of ionizations, directly in or very near to DNA, resulting in clustered initial molecular damage in the DNA, are critical physical features of the tracks [115]. To assess such clustered DNA damage, a categorization of strand breaks into six classes according to the absence or presence of further SSBs and DSBs within a short DNA segment was introduced already in the earliest calculations of DNA strand breaks [56]. This scheme, extended later by considering also base damage and the direct, indirect or mixed origin of the strand breaks, has been adopted in several investigations [57,80,94] to quantify the increasing complexity of DNA lesions with increasing LET. An analysis of DNA strand break clusters has been made with PARTRAC for irradiations with various light ions [17] regarding distributions of energy depositions. Distributions of DSBs in three complexity classes is presented in Fig. 6, where with increasing LET a steep increase of DSBs within clusters of two or more DSBs (*DSB*$^{++}$) is evident, whereas DSBs without additional nearby SSB (*DSB*) and DSBs in clusters with one or more SSBs (*DSB*$^+$) culminate at about 80 and 300 keV/μm LET, respectively.

Base damage due to direct energy deposition onto, or interaction of radicals with, DNA bases contributes significantly to DNA lesion complexity. There are apparently more damaged bases than strand breaks with an estimated ratio of 2–2.4 for both low- and high-LET irradiation [94]. Base damage has been introduced in PARTRAC calculations in the framework of DNA repair simulations (see Section 4.6) since such lesions have been supposed to influence DNA repair kinetics [116]. The relatively small fractions of slowly repairing DSBs suggest that only a subset of base lesions near DNA ends contribute to slowing down the repair processes. In analogy to strand break induction it has been assumed in PARTRAC that such retarding base lesions were formed due to direct effects with a probability increasing linearly from 0 at 0 eV to 1 at (and above) 60 eV deposited energy, and due to indirect effects with 50% probability attributed to •OH interactions with bases [18].

4.5. Cell inactivation

The close correlation between DSBs and cell killing (or cell survival) became evident in the 1980s of the last century [117–119]. The relation between irradiation of cells and cell killing as well as modelling approaches on this issue [120–122] are of fundamental importance due to crucial involvement in radiation therapy and go beyond the scope of this review.

The relation between the observed LET dependence for calculated yields of DSBs of various complexity and cell inactivation has first been studied with PARTRAC for proton and α particle irradiation [16]; a similar investigation for proton irradiation has been made for V79 cells [123]. Experimental datasets of RBE values for cell inactivation of human fibroblast cells have been considered in an extended analysis [17] after irradiation by various ion types [124,125]. The observed RBE values for cell inactivation have a maximum of about 4 between 100 and 200 keV/μm LET, whereas calculated RBE values of DSB^{+} reach a maximum of about 2 at an LET of about 70 keV/μm and DSB^{++} culminate with RBE values above 10 at LET values of about 200 keV/μm. A weighted sum with cell killing probabilities of 8%, 2% and 0.5% for the categories of DSB^{++}, DSB^{+} and DSB, respectively, has been found in overall agreement with the LET dependence of measured RBE and cell inactivation cross sections [17]. The reported studies provide support for a dominant role of DSB complexity in radiation-induced cell killing, however, a contribution of simple DSBs becomes evident in particular for radiation qualities with lower LET.

4.6. DNA repair processes

Recently, the PARTRAC suite has been complemented by a stochastic model describing cellular processes aimed at repairing radiation damage to DNA [18]. The scheme of the repair model (Fig. 7) represents the NHEJ DNA repair pathway which is the dominant DSB repair mechanism in eukaryotic cells during the G1 phase of cell cycle. Processing by NHEJ machinery of the two DNA ends of a DSB is tracked separately within the repair module. The considered characteristics of DNA ends as determined by PARTRAC calculations of initial DNA damage are geometric position, genomic position, fiber length and geometric distance from the DNA end to a nuclear attachment site or to the next DSB for short DNA fragments, DSB complexity (related to one DNA end) in terms of additional nearby strand breaks or base lesions scored up to an undamaged sequence of 20 bp; and the single-stranded overhang length. DNA ends are classified into so-called 'dirty' DNA ends carrying nearby SSB(s) and/or relevant (i.e. contributing to slowing down of the repair process) base lesion(s), and 'clean' DNA ends without such nearby damage; thus, simple DSBs include two clean DNA ends whereas complex DSBs comprise either a dirty and a clean or two dirty DNA ends. After a quick chromatin remodelling and DNA mobilization step, the DNA ends are allowed to diffuse in a step-by-step random walk process, limited by nuclear attachment sites and fragment lengths. In parallel to diffusive motion, attachment of major repair enzymes involved in the NHEJ mechanism is considered [126]. First, Ku70/80 is recruited to the DNA end; alternatively, attachment of other enzymes inhibiting Ku70/80 recruitment may occur. Then a DNA–PK complex is formed by subsequent attachment of the catalytic subunit DNA–PKcs. Two DNA ends with attached DNA–PK undergo synapsis when they are in sufficient vicinity, and then the two DNA–PK complexes cross-phosphorylate each other. Attachment of further NHEJ repair enzymes [126] including ligase IV, XRCC4 and others mediate the repair of nearby base lesions, processing of single-stranded overhangs, filling of gaps and final ligation of the two DNA ends. Failure of the repair process during post-synaptic states leading to a restart of the procedure as well as reaching a state where rejoining is impossible may be taken into account, too. The finally joined ends are classified into correctly rejoined DSBs, formation of rings, chromosomal aberrations, and other forms of misrejoined DNA ends.

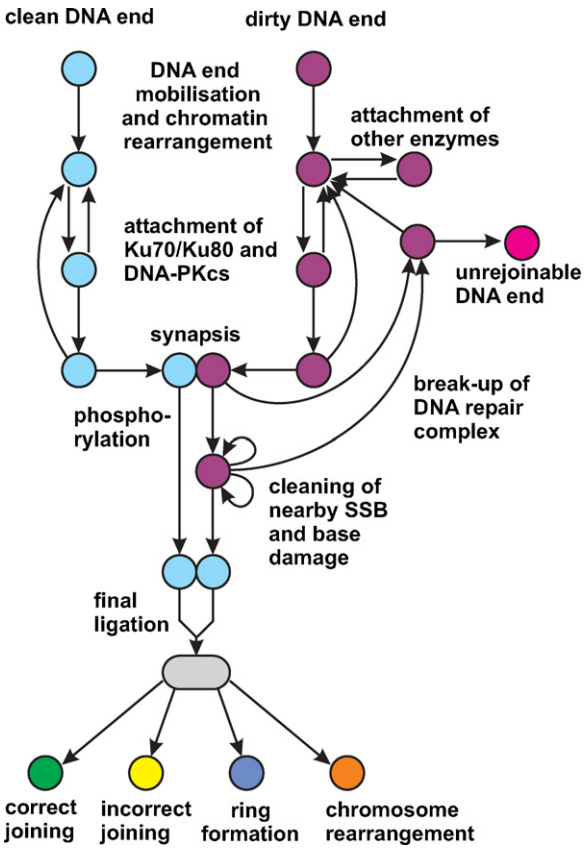

Fig. 7. Scheme for processing of a clean DNA end and a dirty DNA end within the DNA repair model of PARTRAC.

Attachment and detachment of repair enzymes is usually modelled by stochastic change of states in a first-order kinetics approach which is determined by a characteristic time or rate as a single parameter. Characteristic times for enzyme attachment during the pre-synaptic phase have been derived from enzyme kinetics data [127]. Information on enzyme detachment has been inferred from fluorescence recovery after photobleaching data [128]. Such particular information is not yet available for the post-synaptic phase; instead, parameter adaptation to measured DNA repair kinetics has been used. Alternatively, enzyme attachment processes may be modelled as binary interaction of diffusing repair enzymes with DNA ends. This approach, however, needs more parameters including enzyme concentrations, reaction rates with DNA ends, turnover times, and diffusion coefficients, but it allows considering effects of limited availability of enzymes and steps involving enzyme production within the repair process.

An adaptation of model parameters resulted for low-LET irradiation in a reasonable agreement [18] between calculated and measured repair kinetics [129], and calculated dose dependent yields were also found in accord with experimental findings for misrejoined DSB [130] and chromosomal aberrations [131] when diffusion corresponded to measurements of DSB motion [132]; however, the calculations obviously overestimated the fractions of residual DSBs at low doses after long repair times [18].

Application of the repair model to experimental data on DSB rejoining after ion irradiation [133] has revealed the need for some model refinements [134]. The rejoining kinetics after ^{60}Co γ-ray irradiation as low-LET reference [133] which was initially slower but passed then into a smaller slowly rejoining fraction than in

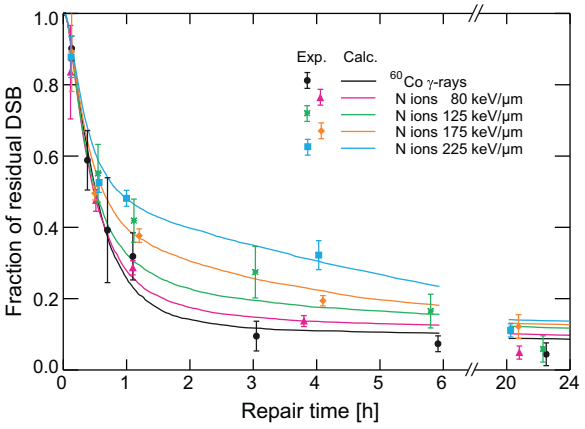

Fig. 8. DSB repair kinetics after 100 Gy irradiation of human fibroblast cells with ^{60}Co γ-rays and nitrogen ions of various LET values. Symbols: experimental results [133], lines: calculations.

the kinetics modelled earlier [129], could be reproduced with a new adaptation of characteristic times during the post-synaptic phase. In order to obtain reasonable agreement also for N ion irradiation with LET values between 80 and 225 keV/μm (Fig. 8), new approaches have been introduced [135]. First, the observed similar initial reduction of residual DSBs after photon and nitrogen ion irradiation could be achieved in calculations with delayed generation of a fraction of DSBs in parallel to initial repair processes. Such a DSB generation has been observed in repair deficient cells using low temperature lysis protocols [136]. Second, agreement with the measured LET-dependence of slowly rejoining DSB fractions and the kinetics during the later repair phase has been considerably improved by an alternative modelling approach with tracking of individual repair enzymes that mediate the removal of nearby lesions. Finally, irreversibly unrejoinable states have been introduced in the model in order to reproduce the observed increase with increasing LET in the fraction of residual DSBs after long repair times.

4.7. Parameter uncertainty and sensitivity

The Monte Carlo approach implemented in PARTRAC inevitably introduces a large number of model parameters. Some of them have been addressed by dedicated experiments or theoretical studies, such as cross sections, diffusion coefficients and reaction rate constants needed for the track structure part, and their uncertainties are usually known from these studies. For other parameters, independent experimental or theoretical investigations are not available. Often, certain values can be excluded as being physically impossible or unrealistic. Generally, however, the parameters are limited only by the requirement to reproduce the experimental data on related end points; e.g. the distance between two SSBs to form a DSB has been inferred from relative yields of SSBs and DSBs. Due to computational expensiveness of these Monte Carlo calculations, optimization methods employed in deterministic modelling approaches have not been used so far; instead, parameter values have been derived by trial-and-error methods, driven by the aim to achieve a reasonable agreement of calculated results with the experiments. Reliably assessing the uncertainty of such parameter estimates is not feasible. Moreover, many parameters, though mechanically distinct, are strongly interrelated, so that a modification of one parameter can be greatly compensated by adapting another one; this is the case e.g. for the effective DNA target volume and the energy needed for SSB induction.

Several studies have been performed in order to determine the most critical parameters and assess the sensitivity of modelling results to their variations. With respect to parameters for the chemical phase of track structure development, the transport of sub-excitation electrons was found to be of particular importance; however, varying the mean transport distance of sub-excitation electrons by ~1/3, corresponding to uncertainties in determination of this parameter from independent studies, has changed the yields of •OH by less than 5% [137]. For SSB induction by direct effects, alternative models of the dependence of SSB induction probability on deposited energy (constant, threshold-type, or linearly increasing probability) lead to rather similar SSB yields [13]; for the threshold-type SSB induction, varying the threshold from 7 to 17.5 eV resulted in a more than twofold difference in the SSB yield [10]. Concerning DSB, increasing the distance between two SSBs for being scored as a DSB from 2 to 10 bp enhanced the DSB yield almost by a factor of 3 [10]; varying the rate of SSB to DSB conversion from 0 to 3% increased the DSB yields by 50–100% [13]. For the NHEJ repair model, available data are not sufficient for uniquely determining the parameter values, i.e. although dealing with mechanistically distinct parameters, they are correlated in terms of data fitting; e.g. a 10-fold change in the rate of Ku attachment may be compensated for by adapting other parameters of the pre-synaptic phase of NHEJ [18].

In addition, one has to keep in mind that the parameter values derived under specific conditions cannot be directly transferred to another cell type, different experimental setup or even to in vivo situation. Moreover, especially because of the parameter correlation issue, picking up a parameter value and using it in other models needs careful consideration.

5. Conclusions

The present suite of PARTRAC tools has demonstrated its capabilities in the calculation of track structures including the physical, physico-chemical and chemical stages as well as the initial radiation damage to cellular DNA. For a prediction of radiation effects on larger scales like cells, tissues or organisms, the recent extension of the temporal dimension from microseconds up to days by more than 10 orders of magnitude is a major step forward. First applications of the combined initial damage and repair models have yielded appealing results; however, improvements and further developments are needed to enable applications of these mechanistic modelling studies in radiation therapy optimization, and to fill the gap towards mechanistic modelling of radiation-induced cancer [3] and other diseases [138] for an application on radiation risks of inexperienced irradiations like long-term manned space missions.

Conflict of interest statement

There are no conflicts of interests.

Acknowledgements

This work was partially supported by the Integrated Projects 'RISC-RAD' (FI6R-CT-2003-508842) and 'NOTE' (FI6R-036465) of the Euratom specific programme for research and training on nuclear energy, 6th FP of the EC. M. Dingfelder acknowledges partial funding from the National Aeronautics and Space Administration (Grant no. NNJ04HF39G).

References

[1] L. Mullenders, M. Atkinson, H. Paretzke, L. Sabatier, S. Bouffler, Assessing cancer risks of low-dose radiation, Nat. Rev. Cancer 9 (2009) 596–604.

[2] D.T. Goodhead, Understanding and characterisation of the risks to human health from exposure to low levels of radiation, Radiat. Prot. Dosimetry 137 (2009) 109–117.
[3] P. Jacob, R. Meckbach, J.C. Kaiser, M. Sokolnikov, Possible expressions of radiation-induced genomic instability, bystander effects or low-dose hypersensitivity in cancer epidemiology, Mutat. Res. 687 (2010) 34–39.
[4] L. Mariotti, A. Facoetti, D. Alloni, A. Bertolotti, E. Ranza, A. Ottolenghi, Effects of ionizing radiation on cell-to-cell communication, Radiat. Res. 174 (2010) 280–289.
[5] P. Kundrat, W. Friedland, P. Jacob, Modelling of intercellular induction of apoptosis in oncogenic transformed cells and radiation effects on the phenomenon, Radiat. Prot. Dosimetry, in press, doi:10.1093/rpd/ncq521.
[6] H. Nikjoo, S. Uehara, D. Emfietzoglou, F.A. Cucinotta, Track-structure codes in radiation research, Radiat. Meas. 41 (2006) 1052–1074.
[7] H.G. Paretzke, Radiation track structure theory, in: G.R. Freeman (Ed.), Kinetics of Nonhomogeneous Processes, Wiley, New York, 1987, pp. 89–170.
[8] H.G. Paretzke, J.E. Turner, R.N. Hamm, R.H. Ritchie, H.A. Wright, Spatial distributions of inelastic events produced by electrons in gaseous and liquid water, Radiat. Res. 127 (1991) 121–129.
[9] S. Henss, H. Paretzke, Biophysical modelling of radiation induced damage in chromosomes, in: K. Chadwick, G. Moschini, M. Varma (Eds.), Biophysical Modelling of Radiation Effects, Adam Hilger, Bristol, Philadelphia, and New York, 1992, pp. 69–76.
[10] W. Friedland, P. Jacob, H.G. Paretzke, T. Stork, Monte Carlo simulation of the production of short DNA fragments by low-linear energy transfer radiation using higher-order DNA models, Radiat. Res. 150 (1998) 170–182.
[11] M. Dingfelder, D. Hantke, M. Inokuti, H.G. Paretzke, Electron inelastic-scattering cross sections in liquid water, Radiat. Phys. Chem. 53 (1998) 1–18.
[12] F. Ballarini, M. Biaggi, M. Merzagora, A. Ottolenghi, M. Dingfelder, W. Friedland, P. Jacob, H.G. Paretzke, Stochastic aspects and uncertainties its the prechemical and chemical stages of electron tracks in liquid water: a quantitative analysis based on Monte Carlo simulations, Radiat. Environ. Biophys. 39 (2000) 179–188.
[13] P. Bernhardt, W. Friedland, P. Jacob, H.G. Paretzke, Modeling of ultrasoft X-ray induced DNA damage using structured higher order DNA targets, Int. J. Mass Spectrom. 223 (2003) 579–597.
[14] M. Dingfelder, M. Inokuti, H.G. Paretzke, Inelastic-collision cross sections of liquid water for interactions of energetic protons, Radiat. Phys. Chem. 59 (2000) 255–275.
[15] W. Friedland, P. Jacob, P. Bernhardt, H.G. Paretzke, M. Dingfelder, Simulation of DNA damage after proton irradiation, Radiat. Res. 159 (2003) 401–410.
[16] W. Friedland, M. Dingfelder, P. Jacob, H.G. Paretzke, Calculated DNA double-strand break and fragmentation yields after irradiation with He ions, Radiat. Phys. Chem. 72 (2005) 279–286.
[17] W. Friedland, P. Jacob, H.G. Paretzke, A. Ottolenghi, F. Ballarini, M. Liotta, Simulation of light ion induced DNA damage patterns, Radiat. Prot. Dosimetry 122 (2006) 116–120.
[18] W. Friedland, P. Jacob, P. Kundrát, Stochastic simulation of DNA double-strand break repair by non-homologous end joining based on track structure calculations, Radiat. Res. 173 (2010) 677–688.
[19] W.B. Li, W. Friedland, E. Pomplun, P. Jacob, H.G. Paretzke, M. Lassmann, C. Reiners, Track structures and dose distributions from decays of ^{131}I and ^{125}I in and around water spheres simulating micrometastases of differentiated thyroid cancer, Radiat. Res. 156 (2001) 419–429.
[20] M.S. Kreipl, W. Friedland, H.G. Paretzke, Time- and space-resolved Monte Carlo study of water radiolysis for photon, electron and ion irradiation, Radiat. Environ. Biophys. 48 (2009) 11–20.
[21] F. Salvat, J.-M. Fernández-Varea, J. Sempau, PENELOPE-2008: A Code System for Monte Carlo Simulations of Electron and Photon Transport, OECD/Nuclear Energy Agency, Issy-les-Moulineaux, 2008.
[22] D.E. Cullen, J.H. Hubbel, L. Kissel, EPDL97 The Evaluated Data Library, '97 version, Lawrence Livermore National Laboratory, 1997.
[23] M. Dingfelder, Cross section calculations in condensed media: charged particles in liquid water, Radiat. Prot. Dosimetry 99 (2002) 23–28.
[24] J.M. Heller Jr., R.N. Hamm, R.D. Birkhoff, L.R. Painter, Collective oscillations in liquid water, J. Chem. Phys. 60 (1974) 3483–3486.
[25] H. Hayashi, N. Watanabe, Y. Udagawa, C.C. Kao, The complete optical spectrum of liquid water measured by inelastic X-ray scattering, Proc. Natl. Acad. Sci. U.S.A. 97 (2000) 6264–6266.
[26] M. Dingfelder, R.H. Ritchie, J.E. Turner, W. Friedland, H.G. Paretzke, R.N. Hamm, Comparisons of calculations with PARTRAC and NOREC: transport of electrons in liquid water, Radiat. Res. 169 (2008) 584–594.
[27] D. Emfietzoglou, F.A. Cucinotta, H. Nikjoo, A complete dielectric response model for liquid water: a solution of the Bethe Ridge problem, Radiat. Res. 164 (2005) 202–211.
[28] D. Emfietzoglou, I. Abril, R. Garcia-Molina, I.D. Petsalakis, H. Nikjoo, I. Kyriakou, A. Pathak, Semi-empirical dielectric descriptions of the Bethe surface of the valence bands of condensed water, Nucl. Instrum. Methods A 266 (2008) 1154–1161.
[29] P. Bernhardt, H.G. Paretzke, Calculation of electron impact ionization cross sections of DNA using the Deutsch–Mark and binary-encounter-Bethe formalisms, Int. J. Mass Spectrom. 223 (2003) 599–611.
[30] M. Michaud, A. Wen, L. Sanche, Cross sections for low-energy (1–100 eV) electron elastic and inelastic scattering in amorphous ice, Radiat. Res. 159 (2003) 3–22.
[31] M. Dingfelder, A. Travia, R.A. McLawhorn, J.L. Shinpaugh, L.H. Toburen, Electron emission from foils and biological materials after proton impact, Radiat. Phys. Chem. 77 (2008) 1213–1217.
[32] L.H. Toburen, S.L. McLawhorn, R.A. McLawhorn, K.D. Carnes, M. Dingfelder, J.L. Shinpaugh, Electron emission from amorphous solid water induced by passage of energetic protons and fluorine ions, Radiat. Res. 174 (2010) 107–118.
[33] ICRU, Stopping powers and ranges for protons and alpha particles, ICRU report 46, International Commission on Radiation Units and Measurements, Bethesda, MD, 1993.
[34] M. Dingfelder, L.H. Toburen, H.G. Paretzke, An effective charge scaling model for ionization of partially dressed helium ions with liquid water, in: The Monte Carlo Method: Versatility Unbounded in a Dynamic Computing World, April 17–21, American Nuclear Society, LaGrange Park IL, Chattanooga TN, 2005.
[35] M. Dingfelder, I.G. Jorjishvili, J.A. Gersh, L.H. Toburen, Heavy ion track structure simulations in liquid water at relativistic energies, Radiat. Prot. Dosimetry 122 (2006) 26–27.
[36] H.W. Barkas, Nuclear Research Emulsions, Academic Press, New York, 1963.
[37] V. Michalik, M. Begusova, E.A. Bigildeev, Computer-aided stochastic modeling of the radiolysis of liquid water, Radiat. Res. 149 (1998) 224–236.
[38] M. Terrissol, Modelling of radiation damage by ^{125}I on a nucleosome, Int. J. Radiat. Biol. 66 (1994) 447–451.
[39] H. Nikjoo, P. O'Neill, M. Terrissol, D.T. Goodhead, Modelling of radiation-induced DNA damage: the early physical and chemical event, Int. J. Radiat. Biol. 66 (1994) 453–457.
[40] J. Meesungnoen, J.P. Jay-Gerin, A. Filali-Mouhim, S. Mankhetkorn, Low-energy electron penetration range in liquid water, Radiat. Res. 158 (2002) 657–660.
[41] J.A. LaVerne, I. Stefanic, S.M. Pimblottt, Hydrated electron yields in the heavy ion radiolysis of water, J. Phys. Chem. A 109 (2005) 9393–9401.
[42] R.N. Hamm, M.G. Stabin, J.E. Turner, Investigation of a Monte Carlo model for chemical reactions, Radiat. Environ. Biophys. 37 (1998) 151–156.
[43] R.M. Noyes, Effects of diffusion rates on chemical kinetics, in: G. Porter (Ed.), Progress in Reaction Kinetics, Pergamon, London, 1963, pp. 129–160.
[44] R.N. Hamm, J.E. Turner, M.G. Stabin, Monte Carlo simulation of diffusion and reaction in water radiolysis—a study of reactant 'jump through' and jump distances, Radiat. Environ. Biophys. 36 (1998) 229–234.
[45] A.M. Kuzin, On the role of DNA in the radiation damage of the cell, Int. J. Radiat. Biol. 6 (1963) 201–209.
[46] UNSCEAR, Sources and Effects of Ionising Radiation, UNSCEAR 2000 Report to the General Assembly, United Nations, New York, 2000.
[47] M.A. Kadhim, D.A. Macdonald, D.T. Goodhead, S.A. Lorimore, S.J. Marsden, E.G. Wright, Transmission of chromosomal instability after plutonium alpha-particle irradiation, Nature 355 (1992) 738–740.
[48] H. Nagasawa, J.B. Little, Induction of sister chromatid exchanges by extremely low doses of alpha-particles, Cancer Res. 52 (1992) 6394–6396.
[49] K. Baverstock, Why do we need a new paradigm in radiobiology? Mutat. Res. 687 (2010) 3–6.
[50] H.H. Rossi, Interpretation of biological response in terms of microdosimetry, Ann. N. Y. Acad. Sci. 161 (1969) 260–271.
[51] A.M. Kellerer, D. Chmelevsky, Concepts of microdosimetry. I. Quantities, Radiat. Environ. Biophys. 12 (1975) 61–69.
[52] ICRU, Microdosimetry, ICRU Report 36, International Commission on Radiation Units and Measurements, Bethesda, MD, U.S.A., 1983.
[53] H. Nikjoo, D.T. Goodhead, D.E. Charlton, H.G. Paretzke, Energy deposition in small cylindrical targets by monoenergetic electrons, Int. J. Radiat. Biol. 60 (1991) 739–756.
[54] H. Nikjoo, D.T. Goodhead, D.E. Charlton, H.G. Paretzke, Energy deposition in small cylindrical targets by ultrasoft X-rays, Phys. Med. Biol. 34 (1989) 691–705.
[55] D.E. Charlton, J.L. Humm, A method of calculating initial DNA strand breakage following the decay of incorporated ^{125}I, Int. J. Radiat. Biol. Relat. Stud. Phys. Chem. Med. 53 (1988) 353–365.
[56] D.E. Charlton, H. Nikjoo, J.L. Humm, Calculation of initial yields of single- and double-strand breaks in cell nuclei from electrons, protons and alpha particles, Int. J. Radiat. Biol. 56 (1989) 1–19.
[57] H. Nikjoo, P. O'Neill, W.E. Wilson, D.T. Goodhead, Computational approach for determining the spectrum of DNA damage induced by ionizing radiation, Radiat. Res. 156 (2001) 577–583.
[58] E. Pomplun, A new DNA target model for track structure calculations and its first application to I-125 Auger electrons, Int. J. Radiat. Biol. 59 (1991) 625–642.
[59] E. Pomplun, M. Terrissol, Low-energy electrons inside active DNA models: a tool to elucidate the radiation action mechanisms, Radiat. Environ. Biophys. 33 (1994) 279–292.
[60] H. Tomita, M. Kai, T. Kusama, Y. Aoki, A. Ito, Monte Carlo simulation of DNA strand breaks induced by monoenergetic electrons using higher-order structure models of DNA, Int. J. Radiat. Biol. 66 (1994) 669–682.
[61] V.Y. Chepel, I.K. Khvostunov, L.A. Mirny, T.A. Talyzina, S.G. Andreev, 3-D computer modelling of chromatin fibres for radiation damage simulation, Radiat. Prot. Dosimetry 52 (1994) 259–263.
[62] W.R. Holley, A. Chatterjee, Clusters of DNA damage induced by ionizing radiation: formation of short DNA fragments. 1. Theoretical modeling, Radiat. Res. 145 (1996) 188–199.
[63] B. Rydberg, W.R. Holley, I.S. Mian, A. Chatterjee, Chromatin conformation in living cells: support for a zig-zag model of the 30 nm chromatin fiber, J. Mol. Biol. 284 (1998) 71–84.

[64] W. Friedland, H.G. Paretzke, F. Ballarini, A. Ottolenghi, G. Kreth, C. Cremer, First steps towards systems radiation biology studies concerned with DNA and chromosome structure within living cells, Radiat. Environ. Biophys. 47 (2008) 49–61.
[65] P. Bernhardt, W. Friedland, R. Meckbach, P. Jacob, H.G. Paretzke, Monte Carlo simulation of DNA damage by low LET radiation using inhomogeneous higher order DNA targets, Radiat. Prot. Dosimetry 99 (2002) 203–206.
[66] A. Valota, F. Ballarini, W. Friedland, P. Jacob, A. Ottolenghi, H.G. Paretzke, Modelling study on the protective role of OH radical scavengers and DNA higher-order structures in induction of single- and double-strand break by gamma-radiation, Int. J. Radiat. Biol. 79 (2003) 643–653.
[67] W. Friedland, P. Jacob, H.G. Paretzke, M. Merzagora, A. Ottolenghi, Simulation of DNA fragment distributions after irradiation with photons, Radiat. Environ. Biophys. 38 (1999) 39–47.
[68] D. Alloni, A. Campa, M. Belli, G. Esposito, A. Facoetti, W. Friedland, M. Liotta, L. Mariotti, H.G. Paretzke, A. Ottolenghi, A Monte Carlo study of the radiation quality dependence of DNA fragmentation spectra, Radiat. Res. 173 (2010) 263–271.
[69] A. Campa, D. Alloni, E. Antonelli, E. Ballarini, M. Belli, V. Dini, G. Esposito, A. Facoetti, W. Friedland, Y. Furusawa, M. Liotta, A. Ottolenghi, H.G. Paretzke, G. Simone, E. Sorrentino, M.A. Tabocchini, DNA fragmentation induced in human fibroblasts by Fe-56 ions: experimental data and Monte Carlo simulations, Radiat. Res. 171 (2009) 438–445.
[70] G. Kreth, J. Finsterle, J. von Hase, M. Cremer, C. Cremer, Radial arrangement of chromosome territories in human cell nuclei: a computer model approach based on gene density indicates a probabilistic global positioning code, Biophys. J. 86 (2004) 2803–2812.
[71] C. Münkel, R. Eils, S. Dietzel, D. Zink, C. Mehring, G. Wedemann, T. Cremer, J. Langowski, Compartmentalization of interphase chromosomes observed in simulation and experiment, J. Mol. Biol. 285 (1999) 1053–1065.
[72] W. Saenger, Principles of Nucleic Acid Structure, Springer-Verlag, New York, 1984.
[73] D. Freifelder, Molecular Biology, Jones and Bartlett, Boston, 1987.
[74] K.O. Greulich, J. Ausio, H. Eisenberg, Nucleosome core particle structure and structural changes in solution, J. Mol. Biol. 186 (1985) 167–173.
[75] S.G. Swarts, M.D. Sevilla, D. Becker, C.J. Tokar, K.T. Wheeler, Radiation-induced DNA damage as a function of hydration I. Release of unaltered bases, Radiat. Res. 129 (1992) 333–344.
[76] G.V. Buxton, C.L. Greenstock, W.P. Helman, A.B. Ross, Critical review of rate constants for reactions of hydrated electrons, hydrogen atoms and hydroxyl radicals (OH/O^-) in aqueous solution, J. Phys. Chem. Ref. Data 17 (1988) 513–885.
[77] J.F. Ward, Factors controlling the radiosensitivity of cellular DNA, in: D.T. Goodhead, P. O'Neill, H.G. Menzel (Eds.), Microdosimetry – An Interdisciplinary Approach, Royal Society of Chemistry, Cambridge, 1997, pp. 57–64.
[78] D.T. Goodhead, Initial events in the cellular effects of ionizing radiations: clustered damage in DNA, Int. J. Radiat. Biol. 65 (1994) 7–17.
[79] H. Nikjoo, D.E. Charlton, D.T. Goodhead, Monte Carlo track structure studies of energy deposition and calculation of initial DSB and RBE, Adv. Space Res. 14 (1994) 161–180.
[80] H. Nikjoo, P. O'Neill, D.T. Goodhead, M. Terrissol, Computational modelling of low-energy electron-induced DNA damage by early physical and chemical events, Int. J. Radiat. Biol. 71 (1997) 467–483.
[81] B. Boudaiffa, P. Cloutier, D. Hunting, M.A. Huels, L. Sanche, Resonant formation of DNA strand breaks by low-energy (3 to 20 eV) electrons, Science 287 (2000) 1658–1660.
[82] K.M. Prise, M. Folkard, B.D. Michael, B. Vojnovic, B. Brocklehurst, A. Hopkirk, I.H. Munro, Critical energies for SSB and DSB induction in plasmid DNA by low-energy photons: action spectra for strand-break induction in plasmid DNA irradiated in vacuum, Int. J. Radiat. Biol. 76 (2000) 881–890.
[83] M. Ljungman, S. Nyberg, J. Nygren, M. Eriksson, G. Ahnström, DNA-bound proteins contribute much more than soluble intracellular compounds to the intrinsic protection against radiation-induced DNA strand breaks in human cells, Radiat. Res. 127 (1991) 171–176.
[84] B.D. Michael, P. O'Neill, Molecular biology. A sting in the tail of electron tracks, Science 287 (2000) 1603–1604.
[85] M.S. Kreipl, W. Friedland, H.G. Paretzke, Interaction of ion tracks in spatial and temporal proximity, Radiat. Environ. Biophys. 48 (2009) 349–359.
[86] D. Alloni, F. Ballarini, M. Belli, A. Campa, G. Esposito, W. Friedland, M. Liotta, A. Ottolenghi, H.G. Paretzke, Modeling of DNA fragmentation induced in human fibroblasts by Fe-56 ions, Adv. Space Res. 40 (2007) 1401–1407.
[87] V.A. Semenenko, R.D. Stewart, Fast Monte Carlo simulation of DNA damage formed by electrons and light ions, Phys. Med. Biol. 51 (2006) 1693–1706.
[88] Y. Hsiao, R.D. Stewart, Monte Carlo simulation of DNA damage induction by X-rays and selected radioisotopes, Phys. Med. Biol. 53 (2008) 233–244.
[89] J. Nygren, M. Ljungman, G. Ahnström, Chromatin structure and radiation-induced DNA strand breaks in human cells: soluble scavengers and DNA-bound proteins offer a better protection against single- than double-strand breaks, Int. J. Radiat. Biol. 68 (1995) 11–18.
[90] K. Hieda, DNA damage induced by vacuum and soft X-ray photons from synchrotron radiation, Int. J. Radiat. Biol. 66 (1994) 561–567.
[91] M.A. Siddiqi, E. Bothe, Single- and double-strand break formation in DNA irradiated in aqueous solution: dependence on dose and OH radical scavenger concentration, Radiat. Res. 112 (1987) 449–463.
[92] K.M. Prise, G. Ahnström, M. Belli, J. Carlsson, D. Frankenberg, J. Kiefer, M. Löbrich, B.D. Michael, J. Nygren, G. Simone, B. Stenerlöw, A review of DSB induction data for varying quality radiations, Int. J. Radiat. Biol. 74 (1998) 173–184.
[93] C.M. de Lara, M.A. Hill, T.J. Jenner, D. Papworth, P. O'Neill, Dependence of the yield of DNA double-strand breaks in Chinese hamster V79-4 cells on the photon energy of ultrasoft X rays, Radiat. Res. 155 (2001) 440–448.
[94] H. Nikjoo, P. O'Neill, M. Terrissol, D.T. Goodhead, Quantitative modelling of DNA damage using Monte Carlo track structure method, Radiat. Environ. Biophys. 38 (1999) 31–38.
[95] D. Frankenberg, H.J. Brede, U.J. Schrewe, C. Steinmetz, M. Frankenberg-Schwager, G. Kasten, E. Pralle, Induction of DNA double-strand breaks by ^1H and ^4He ions in primary human skin fibroblasts in the LET range of 8 to 124 keV/μm, Radiat. Res. 151 (1999) 540–549.
[96] B. Rydberg, L. Heilbronn, W.R. Holley, M. Löbrich, C. Zeitlin, A. Chatterjee, P.K. Cooper, Spatial distribution and yield of DNA double-strand breaks induced by 3–7 MeV helium ions in human fibroblasts, Radiat. Res. 158 (2002) 32–42.
[97] E. Höglund, DNA Fragmentation in Cultured Cells Exposed to High Linear Energy Transfer Radiation, Comprehensive Summaries of Uppsala Dissertations from the Faculty of Medicine 960, Uppsala, 2000.
[98] A. Brahme, B. Rydberg, P. Blomquist, Dual spatially correlated nucleosomal double strand breaks in cell inactivation, in: D. Goodhead, P. O'Neill, H.G. Menzel (Eds.), Microdosimetry – An Interdisciplinary Approach, The Royal Society of Chemistry, Cambridge, 1997, pp. 125–128.
[99] B. Rydberg, Clusters of DNA damage induced by ionizing radiation: formation of short DNA fragments.2. Experimental detection, Radiat. Res. 145 (1996) 200–209.
[100] S.E. Gerchman, V. Ramakrishnan, Chromatin higher-order structure studied by neutron scattering and scanning transmission electron microscopy, Proc. Natl. Acad. Sci. U.S.A. 84 (1987) 7802–7806.
[101] S.P. Williams, J.P. Langmore, Small angle X-ray scattering of chromatin radius and mass per unit length depend on linker length, Biophys. J. 59 (1991) 606–618.
[102] V.E. Cook, R.K. Mortimer, A quantitative model of DNA fragments generated by ionizing radiation, and possible experimental applications, Radiat. Res. 125 (1991) 102–106.
[103] M. Löbrich, P.K. Cooper, B. Rydberg, Non-random distribution of DNA double-strand breaks induced by particle irradiation, Int. J. Radiat. Biol. 70 (1996) 493–503.
[104] H.C. Newman, K.M. Prise, M. Folkard, B.D. Michael, DNA double-strand break distributions in X-ray and alpha-particle irradiated V79 cells: evidence for non-random breakage, Int. J. Radiat. Biol. 71 (1997) 347–363.
[105] H. Höglund, B. Stenerlöw, Induction and rejoining of DNA double-strand breaks in normal human skin fibroblasts after exposure to radiation of different linear energy transfer: possible roles of track structure and chromatin organization, Radiat. Res. 155 (2001) 818–825.
[106] M. Belli, R. Cherubini, M. Dalla Vecchia, V. Dini, G. Esposito, G. Moschini, O. Sapora, C. Signoretti, G. Simone, E. Sorrentino, M.A. Tabocchini, DNA fragmentation in mammalian cells exposed to various light ions, Adv. Space Res. 27 (2001) 393–399.
[107] A. Campa, F. Ballarini, M. Belli, R. Cherubini, V. Dini, G. Esposito, W. Friedland, S. Gerardi, S. Molinelli, A. Ottolenghi, H. Paretzke, G. Simone, M.A. Tabocchini, DNA DSB induced in human cells by charged particles and gamma rays: experimental results and theoretical approaches, Int. J. Radiat. Biol. 81 (2005) 841–854.
[108] I.K. Khvostunov, S.G. Andreev, Y. Eidelman, Biophysical analysis of radiation induced initial DNA fragmentation, Radiat. Prot. Dosimetry 99 (2002) 151–152.
[109] A. Campa, G. Esposito, M. Belli, G. Simone, M.A. Tabocchini, DNA fragmentation in V79 cells irradiated with light ions as measured by pulsed-field gel electrophoresis II. Simulation with a generalized broken stick model, Int. J. Radiat. Biol. 80 (2004) 229–238.
[110] A.L. Ponomarev, F.A. Cucinotta, R.K. Sachs, D.J. Brenner, Monte Carlo predictions of DNA fragment-size distributions for large sizes after HZE particle irradiation, Phys. Med. 17 (Suppl. 1) (2001) 153–156.
[111] R.K. Sachs, A.L. Ponomarev, P. Hahnfeldt, L.R. Hlatky, Locations of radiation-produced DNA double strand breaks along chromosomes: a stochastic cluster process formalism, Math. Biosci. 159 (1999) 165–187.
[112] M. Pinto, H.C. Newman, K.M. Prise, B.D. Michael, Quantification of DNA damage by PFGE: development of an analytical approach to correct for the background distribution, Int. J. Radiat. Biol. 76 (2000) 741–748.
[113] A.L. Ponomarev, M. Belli, P.J. Hahnfeldt, L. Hlatky, R.K. Sachs, F.A. Cucinotta, A robust procedure for removing background damage in assays of radiation-induced DNA fragment distributions, Radiat. Res. 166 (2006) 908–916.
[114] A.L. Ponomarev, M. Belli, P.J. Hahnfeldt, L. Hlatky, R.K. Sachs, F.A. Cucinotta, Subtraction of background damage in PFGE experiments on DNA fragment-size distributions, Radiat. Environ. Biophys. 46 (2007) 155–160.
[115] D.T. Goodhead, J. Thacker, R. Cox, Weiss lecture. Effects of radiations of different qualities on cells: molecular mechanisms of damage and repair, Int. J. Radiat. Biol. 63 (1993) 543–556.
[116] A. Asaithamby, N. Uematsu, A. Chatterjee, M.D. Story, S. Burma, D.J. Chen, Repair of HZE-Particle-induced DNA double-strand breaks in normal human fibroblasts, Radiat. Res. 169 (2008) 437–446.
[117] G.W. Barendsen, RBE-LET relationships for different types of lethal radiation damage in mammalian cells: comparison with DNA DSB and an interpretation of differences in radiosensitivity, Int. J. Radiat. Biol. 66 (1994) 433–436.
[118] I.R. Radford, Evidence for a general relationship between the induced level of DNA double-strand breakage and cell-killing after X-irradiation of mam-

malian cells, Int. J. Radiat. Biol. Relat. Stud. Phys. Chem. Med. 49 (1986) 611–620.
[119] K.M. Prise, S. Davies, B.D. Michael, The relationship between radiation-induced DNA double-strand breaks and cell kill in hamster V79 fibroblasts irradiated with 250 kVp X-rays 2. 3 MeV neutrons or ^{238}Pu alpha-particles, Int. J. Radiat. Biol. Relat. Stud. Phys. Chem. Med. 52 (1987) 893–902.
[120] M. Scholz, T. Elsässer, Biophysical models in ion beam radiotherapy, Adv. Space Res. 40 (2007) 1381–1391.
[121] C.K. Wang, The progress of radiobiological models in modern radiotherapy with emphasis on the uncertainty issue, Mutat. Res. 704 (2010) 175–181.
[122] P. Kundrat, Detailed analysis of the cell-inactivation mechanism by accelerated protons and light ions, Phys. Med. Biol. 51 (2006) 1185–1199.
[123] P. Kundrat, R.D. Stewart, On the biophysical interpretation of lethal DNA lesions induced by ionising radiation, Radiat. Prot. Dosimetry 122 (2006) 169–172.
[124] R. Cox, W.K. Masson, Mutation and inactivation of cultured mammalian cells exposed to beams of accelerated heavy ions. III. Human diploid fibroblasts, Int. J. Radiat. Biol. Relat. Stud. Phys. Chem. Med. 36 (1979) 149–160.
[125] C. Tsuruoka, M. Suzuki, T. Kanai, K. Fujitaka, LET and ion species dependence for cell killing in normal human skin fibroblasts, Radiat. Res. 163 (2005) 494–500.
[126] M.R. Lieber, Y. Ma, U. Pannicke, K. Schwarz, Mechanism and regulation of human non-homologous DNA end-joining, Nat. Rev. Mol. Cell Biol. 4 (2003) 712–720.
[127] A. Taghva, Y. Ma, M.R. Lieber, Analysis of the kinetic and equilibrium binding of Ku protein to DNA, J. Theor. Biol. 214 (2002) 85–97.
[128] N. Uematsu, E. Weterings, K. Yano, K. Morotomi-Yano, B. Jakob, G. Taucher-Scholz, P.O. Mari, D.C. van Gent, B.P. Chen, D.J. Chen, Autophosphorylation of DNA–PK_{CS} regulates its dynamics at DNA double-strand breaks, J. Cell Biol. 177 (2007) 219–229.
[129] K.H. Karlsson, I. Radulescu, B. Rydberg, B. Stenerlöw, Repair of radiation-induced heat-labile sites is independent of DNA–PKcs, XRCC1 and PARP, Radiat. Res. 169 (2008) 506–512.
[130] B. Rydberg, B. Cooper, P.K. Cooper, W.R. Holley, A. Chatterjee, Dose-dependent misrejoining of radiation-induced DNA double-strand breaks in human fibroblasts: experimental and theoretical study for high- and low-LET radiation, Radiat. Res. 163 (2005) 526–534.
[131] E. Nasonova, K. Fussel, S. Berger, E. Gudowska-Nowak, S. Ritter, Cell cycle arrest and aberration yield in normal human fibroblasts I. Effects of X-rays and 195 MeV/u C ions, Int. J. Radiat. Biol. 80 (2004) 621–634.
[132] B. Jakob, J. Splinter, M. Durante, G. Taucher-Scholz, Live cell microscopy analysis of radiation-induced DNA double-strand break motion, Proc. Natl. Acad. Sci. U.S.A. 106 (2009) 3172–3177.
[133] B. Stenerlöw, E. Höglund, J. Carlsson, E. Blomquist, Rejoining of DNA fragments produced by radiations of different linear energy transfer, Int. J. Radiat. Biol. 76 (2000) 549–557.
[134] W. Friedland, P. Jacob, P. Kundrát, Mechanistic simulation of radiation damage to DNA and its repair: on the track towards systems radiation biology modelling, Radiat. Prot. Dosimetry, in press, doi:10.1093/rpd/ncq383.
[135] W. Friedland, P. Kundrát, P. Jacob, Stochastic modelling of DSB repair after photon and ion irradiation, Int. J. Radiat. Biol., submitted for publication.
[136] S.K. Singh, W.Z. Wu, W.Q. Wu, M.L. Wang, G. Iliakis, Extensive repair of DNA double-strand breaks in cells deficient in the DNA–PK-dependent pathway of NHEJ after exclusion of heat-labile sites, Radiat. Res. 172 (2009) 152–164.
[137] M.S. Kreipl, Biophysikalische Transportrechnungen: Einfluss von Intertrack-Effekten in Ionenspuren auf die Ausbeuten biologischer Endpunkte und Auswirkungen von Coulomb-Kräften innerhalb einer Ionenspur auf die Radiolyse von Wasser, Diplomarbeit (in German), TU Munich, 2007.
[138] M.P. Little, A. Gola, I. Tzoulaki, A model of cardiovascular disease giving a plausible mechanism for the effect of fractionated low-dose ionizing radiation exposure, PLoS Comput. Biol. 5 (2009) e1000539.